39th AIAA/ASME/SAE/ASEE Joint Propulsion Conference and Exhibit
Huntsville, Alabama, 20 - 23 Jul 2003

CAVITATION AND ROTORDYNAMICS ACTIVITIES AT CENTROSPAZIO

Emilio Rapposelli** and Luca d'Agostino*

Centrospazio – Consorzio Pisa Ricerche, 56121 Ospedaletto, Pisa, Italy

Centrospazio has long been carrying out an articulated program of experimental, theoretical and numerical research on cavitation and two-phase flow dynamics in connection with liquid propellant rocket fuel feed systems. The areas of involvement dealt with in recent years range from the modeling and simulation of cavitation to the study of rotordynamic fluid forces in whirling and cavitating axial inducers and journal bearings. Specifically, this paper illustrates the development of a new cavitation model accounting in an approximate but physical way for the occurrence of thermal cavitation and liquid quality effects, and the realization of the CPRTF (Cavitating Pump Rotordynamic Test Facility), a water loop for the measurement of rotordynamic fluid forces on whirling and cavitating turbopump impellers, and the TCT (Thermal Cavitation Tunnel), a modified version of the CPRTF for cavitation experiments in fluid dynamic and thermal cavitation similarity. Representative results of the application of cavitation model to journal bearings, hydrofoils and helical inducers and the typical performance of the CPRTF and TCT are presented.

Nomenclature

Latin symbols

a	sound speed
b	bubble semi-separation, blade height
c	chord
C	bearing clearance
C_p	pressure coefficient
e	eccentricity
d_S	specific diameter
f	nondimensional impeller force, frequency
$\mathbf{F}$	nondimensional bearing force
H	height of the lubricating film
i	imaginary unit
K_C	cavitation parameter
L	bearing length
M	Mach number
m	mass
$\dot{m}$	mass flow rate
n	no. of active nuclei per unit liquid volume
N_B	number of blades
N_R	number of blade revolutions
p	pressure
P	blade axial pitch
Q_{vap}	heat of vaporization
$\dot{Q}$	volumetric flow rate
r	radius , radial coordinate
Re	Reynolds number
T	temperature
$\boldsymbol{u}$	velocity vector
V	volume
X_g	noncondensable gas fraction
x, y	lateral coordinates
z	axial coordinate

Greek symbols

α	volume fraction, void fraction
α_T	thermal diffusivity
β	blade angle
δ	cavitation layer thickness
δ_T	thermal boundary layer thickness
ε	volume fraction, relative eccentricity
ϑ	azimuthal coordinate, angle of attack
ζ	nondimensional damping coefficient
μ	Newtonian viscosity
ν	kinematic viscosity
ρ	density
σ	Euler cavitation number
φ	velocity potential
ω	rotational speed
Ω	whirl speed
Ω_S	pump specific

Subscripts

C	cavitation
H	hub
L	liquid
R	radial
sat	saturation
t	total
T	tip, tangential
V	vapor
1	pump inlet station
2	pump outlet station

Introduction

Propellant feed turbopumps are a crucial component of all primary propulsion concepts powered by liquid propellant rocket engines because of the severe limitations associated with the design of high power density, dynamically stable machines capable of meeting the extremely demanding suction, pumping and reliability requirements of space transportation systems (Stripling & Acosta, 1962). In most cases these pumps employ an inducer upstream of the centrifugal stage(s) in order to improve the

** Research Engineer, Centrospazio, AIAA Member; e.rapposelli@cpr.it.

* Professor, Department of Aerospace Engineering, AIAA Member

suction performance and reduce the propellant tank pressure and weight. Significant cavitation levels typically occur in inducers and often lead to the development of flow instabilities that can seriously degrade the performance of the machine, or even cause its rapid failure.

The occurrence of rotating cavitation has been extensively reported in the development of most high performance liquid propellant rocket fuel feed systems, including the Space Shuttle Main Engine (Ryan et al. 1994), the Ariane 5 engine (Goirand et al. 1992) and the LE-7 engine (Kamijo, Yoshida & Tsujimoto 1993; Tsujimoto et al. 1997). In particular, in modern inducers rotating cavitation is becoming a major concern in addition to cavitation surge. It has been found that rotating cavitation is caused by positive values of the pump's mass flow gain factor, which also causes cavitation surge.

Recently Tsujimoto and Semenov (2002) identified a new surge-mode (axial) instability with frequency as high as 4 to 5 times the rotational frequency in the turbopump inducers of the H-II and H-II-A Japanese rocket engines. Since conventional cavitation surge typically occurs at much lower frequencies (Brennen, 1994), this new instability has been called "high order surge-mode instability". According to the authors its unforeseen resonance with the first bending mode of the inducer blades was responsible for the fatigue failure of the liquid hydrogen pump inducer of the 8th launch of H-II rocket (NASDA Report No. 94, May 2000, NASDA Report No. 96, June 2000).

More generally, supersynchronous and subsynchronous shaft vibrations have been experienced in the Shuttle main engine and in the Arianne 5 engine turbopumps and these dramatically confirmed that the combined effects of rotordynamic fluid forces and cavitation represent the dominant fluid mechanical phenomena that adversely affect the dynamic stability and pumping performance of high power density turbopumps (Brennen, 1994).

Available evidence clearly indicates that the current trend towards supercritical operation of turbopumps for liquid propellant feed systems imposes careful reconsideration of the contributions of rotordynamic fluid forces on cavitating impellers in determining the dynamic properties of the rotors. Simple overestimation of these forces with reference to noncavitating operation is just not acceptable in supercritical machines since it would lead to unrealistically low values of the critical speeds and to drastic overestimates of the stability margins in the real operating conditions, where significant cavitation is usually accepted.

Typical liquid propellants for space launchers are fluids with relatively high vapor pressures. In these fluids the changes of the vapor pressure in growing cavities due to the heat absorbed by evaporation phenomena at the phase interfaces (thermal cavitation) are known to represent the dominant source of important cavitation scaling effects. Efficient semi-empirical laws have been developed to predict the impact of thermal effects on the steady suction performance of cavitating turbopumps. On the other hand, practically no systematic information is available to date on the influence of thermal effects on unsteady cavitation instabilities. In addition, there are reasons to believe that the laws developed for scaling thermal effects in steady conditions may no longer be applicable in the presence of rapid and unsteady flow instabilities of cavitating turbopumps.

In most practical situations, the complexity of the physical phenomena involved and the uncertain knowledge of the actual flow conditions clearly indicate that theoretical and numerical analyses alone are still of limited value for accurate prediction of cavitation-induced turbopump instabilities, and must be associated with detailed experimentation on scaled models. To this purpose Centrospazio has recently developed a low-cost, versatile and easily instrumentable test facility, which can be presently arranged in three alternative configurations:

1. The CPTF, Cavitating Pump Test Facility, designed for general experimentation on cavitating/non-cavitating turbopumps under fluid dynamic and thermal cavitation similarity;
2. The CPRTF, Cavitating Pump Rotordynamic Test Facility (Rapposelli, Cervone, Bramanti & d'Agostino, 2002), an upgraded version of the CPTF also capable of investigating rotordynamic fluid forces in forced vibration experiments on turbopumps whose impeller axis rotates with adjustable eccentricity and sub-synchronous or super-synchronous whirl speed;
3. The TCT, Thermal Cavitation Tunnel (Rapposelli, Cervone, Bramanti & d'Agostino, 2003), an alternative configuration of the CPTF specifically designed for the investigation of 2D or 3D cavitating flows over test bodies in thermal similarity conditions.

Theoretical Investigations

A major difficulty in the analysis of cavitating flows is the presence of free surfaces, whose shape, location and evolution are not known "a priori" and must in principle be obtained as part of the solution of the flow field. Therefore cavitation poses formidable obstacles in terms of both physical and numerical modeling.

Successful development of a model for simulating cavitation in technical applications must be based on careful consideration of the final objectives and implementation constraints, in order to exploit all opportunities to simplify the formulation of the

problem by including only the essential physical phenomena. Typical analyses of propellant feed turbopumps for space applications put especial prize on the prediction of the suction and dynamic performances of the machine, which are essentially related to the macroscopic characteristics of the flow field. These considerations suggest to develop an equivalent fluid model where the fine details of the cavity growth and collapse are neglected, and the cavitating flow is visualized in terms of a single fluid, whose properties are obtained by introducing suitable simplifying assumptions.

Cavitation Modeling

Considering that adiabatic force-free flows of cavitating liquids are practically isenthalpic and that the thermal term dominates the kinetic, viscous and unsteady contributions in the enthalpy equation, it is possible to use the energy balance of the mixture to relate density (or, equivalently, the void fraction) to the local value of the pressure. In this approximation therefore the flow is barotropic, which represents a significant advantage of the isenthalpic formulation, as it reduces the order of the differential problem governing the flow field. Using the previous consideration, a quasi-homogeneous liquid/vapor model, suitably modified to account for thermal effects, has been developed and used to describe the occurrence of flow cavitation in several numerical and analytical analyses (Rapposelli and d'Agostino, 2001 and 2002). The proposed model treats the fully-wetted and two-phase portions of the fluid in a unified manner in order to avoid the use of "ad hoc" matching conditions, whose applicability and accuracy is questionable in flows where significant inertial and/or unsteady effects are present, a situation that is likely to occur in turbopumps for space applications.

In accordance with Brennen's original formulation (1995), in order to account for thermal cavitation effects it is assumed that thermodynamic equilibrium is only established with fraction $0 \le \varepsilon_L \le 1$ and $0 \le \varepsilon_V \le 1$ of the total volume of the liquid and vapor phases:

$$V = (1-\varepsilon_L)V_L + \varepsilon_L V_L + (1-\varepsilon_V)V_V + \varepsilon_V V_V$$

It follows that the sound speed in the cavitating mixture is expressed in terms of the void fraction $\alpha = \alpha_V = 1-\alpha_L$ by:

$$\frac{1}{\rho a^2} = \frac{1-\alpha}{p}\left[(1-\varepsilon_L) f_L + \varepsilon_L g_L\right] + \frac{\alpha}{p}\left[(1-\varepsilon_V) f_V + \varepsilon_V g_V\right]$$

where f_L, g_L, f_V, g_V are known functions of the pressure. It can also be shown that for most fluids $f_V \cong g_V$, so that only ε_L is practically relevant. In particular, for bubbly cavitating flows ($\alpha < 1$) the value of ε_L can be readily estimated in terms of the characteristic values of the bubble radius, R, the bubble separation, b, and the thickness, δ_T, of the thermal boundary layer in the liquid surrounding the bubble interface. Then, using $\alpha \approx R^3/b^3$:

$$\varepsilon_L \cong \frac{(R+\delta_T)^3 - R^3}{b^3 - R^3} = \frac{R^3}{b^3 - R^3}\left[\left(1+\frac{\delta_T}{R}\right)^3 - 1\right] \cong \frac{\alpha}{1-\alpha} B$$

In the thermally-controlled growth of a cavitating spherical bubble $\delta_T \cong \sqrt{\alpha_{TL} t}$ and $R \cong R^* \sqrt{t}$, where α_{TL} is the thermal diffusivity of the liquid. Therefore δ_T / R is approximately constant and can be considered as a free flow parameter, which determines the value of ε_L and accounts for the influence of thermal cavitation effects. Clearly δ_T / R ranges from zero in frozen flows to $\delta_T / R >> 1$ in isothermal equilibrium flows.

Clearly ε_L must level up to unity for any given value of δ_T / R as $\alpha \to 1$ and the above expression is only valid for void fractions not exceeding the value corresponding to $\varepsilon_L = 1$. Hence, with a minor approximation, ε_L is taken equal to the λ-th order harmonic mean:

$$\varepsilon_L = \left[\left(\frac{\alpha}{1-\alpha} B\right)^{-\lambda} + 1\right]^{-1/\lambda}$$

of the limit expressions of ε_L for low and high void fractions. In this equation, consistently with the present model, it can be shown that $\lambda \cong 3$ for the overlap of the thermal boundary layers of neighboring bubbles to occur for a radius change $\Delta R \approx \delta_T$. This formulation provides a smooth transition between the two expressions of ε_L, as expected in real flows as a consequence of the gradual overlapping of the thermal boundary layers.

The value of $\delta_T / R \cong \sqrt{\alpha_{TL}} / R^*$ can also be estimated from $R^* = \left(-C_{p_{\min}} - \sigma\right) U_o^2 / \Sigma(T)$ as a function of the reference flow velocity U_o, the cavitation number $\sigma = (p_o - p_{\text{sat}}) / \frac{1}{2}\rho_L U_o^2$, the minimum pressure coefficient $C_{p\min}$, and the thermodynamic parameter $\Sigma(T) = \rho_{\text{sat}}^2 Q_{\text{vap}}^2 / \rho_L^2 c_{pL} T \sqrt{\alpha_{TL}}$ (Brennen 1995). However, the value of R^* for a single bubble is clearly overestimated, since the presence of multiple bubbles reduces their growth rate. In the present approximation, from the combined-phase continuity and momentum equations of the mixture it follows that two cavitating flows (indexes 1 and 2) with the same boundary conditions have equal velocity and pressure fields if $\alpha_1 = \alpha_2$. Therefore, since $nR^3 \cong \alpha/(1-\alpha)$ where n is the number of active cavitation nuclei per unit liquid volume, it follows that:

$$\frac{R_2^*}{R_1^*} = \frac{R_2}{R_1} = \left[\frac{n_1 \alpha_2 (1-\alpha_1)}{n_2 \alpha_1 (1-\alpha_2)}\right]^{1/3} = \left(\frac{n_1}{n_2}\right)^{1/3}$$

For the flow with a single bubble $n_1 \cong 1/V_C$, where V_C is the cavitation volume ($p \le p_{\text{sat}}$) of the flow. Corrected values of $\delta_T / R \cong \sqrt{\alpha_{TL}} / R_2^*$ for cavitation in waters near room conditions with typical values of

the concentrations of active nuclei (10 to 100 cm^{-3}) are consistent with the estimates of δ_T/R obtained by fitting numerical simulations of the cavitating flow with the available experimental data. Extrapolation to higher temperatures is more uncertain, presumably because of the temperature dependence of the active nuclei concentration.

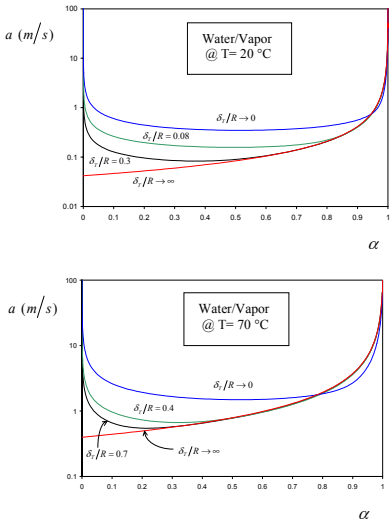

Figure 1. Sonic velocities as a function of the void fraction α for bubbly water/vapor mixtures at 20 °C and 70 °C and several values of δ_T/R computed numerically with order harmonic $\lambda = 3$.

Figure 1 shows the sound speed of a liquid/vapor mixture as functions of the void fraction for water at 20 and 70 °C for several values of δ_T/R. Values of δ_T/R between 0.3 and 0.7 have been found to be the most realistic by comparing numerical simulations with experimental data and have been used in the following calculations. Figure 1 also shows that the sound speed drops by several orders of magnitude to extremely low values even for moderate void fractions. It follows that in cavitating flows both nearly incompressible zones (pure liquid) and regions where the flow may easily become highly supersonic (liquid-vapor mixtures) are present and need to be solved simultaneously. The resulting stiffness of the numerical problem is further increased both by the high density ratio between the two phases (for water at 20 °C the liquid-to-vapor density ratio is on the order of 10^5) and by the strong shock discontinuities occurring in the recondensation at the cavity closure.

Cavitating inducers

Recent theoretical work on turbomachinery was aimed at the understanding the impact of attached blade cavitation on the rotordynamic forces exerted by the fluid on the impeller of whirling turbopumps (d'Agostino & Venturini Autieri, 2002). The available experimental evidence indicates that cavitation reduces the magnitude of the rotordynamic fluid forces, significantly affecting the added mass of the rotor. It is worth nothing that the consequent increase of the critical speeds is of special relevance to highly-loaded supercritical machines, as commonly used in liquid propellant rocket feed systems. A second major effect of cavitation is the introduction of a complex oscillatory dependence of the rotordynamic fluid forces on the whirl frequency (Bhattacharyya 1994). This finding seemed to indicate the possible occurrence of resonance phenomena in the compressible cavitating flow inside the blade channels under the excitation imposed by the eccentric motion of the rotor. Earlier theoretical analyses have addressed the case of infinitely-long whirling helical inducers with uniformly distributed travelling bubble cavitation (d'Auria et al., 1995; d'Agostino and d'Auria, 1997; d'Agostino, d'Auria and Brennen 1998). The results confirmed the presence of internal flow resonances and indicate that bubble dynamic effects do not play a major role, except, perhaps, at extremely high whirl speeds.

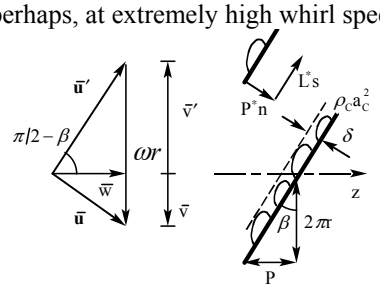

Figure 2. Schematic of the thin layer of attached cavitation pockets on the suction sides of the inducer blades

Following up on this work, the dynamics of the unsteady three-dimensional flow in finite-length helical inducers with attached blade cavitation has been investigated. The linearized governing equations and boundary conditions for a cavitating helical inducer rotating at constant angular speed ω and whirling about the stator axis with constant eccentricity e and angular speed Ω have been solved by separation of variables. Thin blades with constant hub and tip radii, r_H and r_T, have been assumed. Cavitation is thought to occur on the suction sides of the blades (as schematically illustrated in Figure 2) in the form of slowly-moving attached pockets uniformly distributed in a thin layer of given thickness $\delta << P$ and damped acoustic admittance $\rho_C a_C^2(1+i\zeta)$, where ζ is the non-dimensional damping coefficient. The (real) acoustic admittance $\rho_C a_C^2$ has been estimated from the isenthalpic cavitation by assuming reasonable values of the void fraction, and appears in the model through the parameter describing the behavior of the cavitating layer:

$$K_C = \frac{\rho_L \delta P^*}{\rho_C a_C^2 (1+i\zeta)}$$

where $P^* = (P/N_B)\cos\beta$ is the width of the blade channels.

In spite of the simplifications introduced in order to obtain an efficient closed form solution, comparison with the available experimental data indicates that the this theory correctly predicts some of the observed features of the rotordynamic fluid forces in cavitating inducers. The results confirmed the occurrence of internal flow resonances introduced by cavitation. The waterfall plots of Figure 3 clearly show that cavitation intensity, measured by the value of $\mathrm{Re}\{K_C\omega^2\}$, has a major impact in locating the critical speeds and determining the magnitude of the rotordynamic forces as functions of the whirl speed. Two sets of symmetric subsynchronous-supersynchronous resonances are predicted. At higher values of the cavitation parameter the intensities of the resonant peaks decrease and their frequencies approach synchronous conditions. Unstable frequency components with these properties have actually been observed in the vibration spectra of the SSME turbopumps (Zoladz, 2002) under cavitating conditions.

These investigations of rotordynamic forces in whirling and cavitating inducers represents the first theoretical analyses on this subject and yielded very significant results, clearly showing that the behavior of lateral whirl forces is strictly connected with the two-phase nature of the flow and providing useful practical indications and fundamental understanding of its dependence on the relevant flow conditions and parameters.

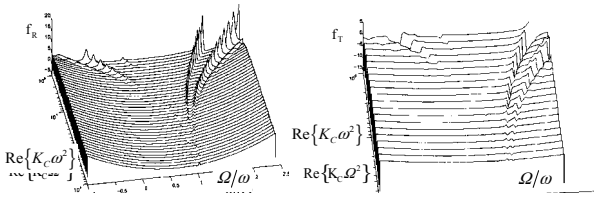

Figure 3. Waterfall plots of the nondimensional rotordynamic forces f_R, f_T on the test inducer as a function of the ratio Ω/ω of the whirl and rotational speeds and the real part of the nondimensional cavitation parameter, $K_C\omega^2$. The flow coefficient is $\phi = 0.0583$, the nondimensional damping coefficient is $\zeta = 0.045$ and the effective length of the blade channels is. $N_R = 0.285$.

Numerical Simulations

Hydrodynamics Bearings

The isenthalpic two-phase flow approximation has been applied to the study of cavitation and ventilation effects in plane journal bearings with whirling eccentricity. In this case a non-linear analysis that accounts for the inertia of the lubricant is used to determine the reaction forces caused by the shaft's eccentric motion both in the viscosity-dominated regime and at intermediate values of the Reynolds number, where the inertia of the lubricant is no longer negligible. The classical iteration method for the Reynolds lubrication equation (Muster and Sternlicht, 1965; Mori and Mori, 1991; Reinhardt and Lund, 1975) has been extended to the unsteady two-phase flow case in order to account for flow acceleration effects in the presence of cavitation and/or ventilation. Significant deviations from the steady-state case have been obtained at moderately high Reynolds numbers ($\mathrm{Re} = \omega Rc/\nu_L \cong 10$).

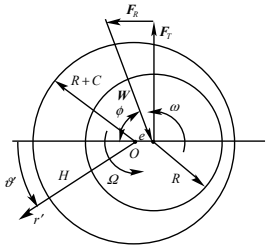

Figure 4. Schematic of the bearing configuration and forces.

Table 1. Reference Bearing Parameters

Shaft radius	$R = 0.05$ m
Relative clearance	$C/R = 2.9\cdot10^{-3}$
Relative eccentricity	$\varepsilon = e/C = 0.6$
Shaft rotational speed	$\omega = 48.1$ rad/s
Shaft whirl speed	$\Omega = 0$ rad/s
Lubricant temperature	$T_L = 70$ °C
Lubricant saturation pressure	$p_{sat} \cong 35$ kPa
Lubricant density	$\rho_L = 1000$ kg/m^3
Lubricant viscosity	$\mu_L = 0.0127$ Pa s
Modified Reynolds number	$\mathrm{Re}^* = \omega C^2/\nu_L = 0.08$
Bearing number	$\Lambda = 0.009$ N
Gas mass fraction in the cavities	$X_g = 0.1$
Alternative flow conditions:	
average void fraction	$\bar{\alpha} = 0.154$
injection pressure @ $\vartheta'_{inj} = 0°$	$p_{inj} = 100$ kPa

In the coordinates r', ϑ', centered in O on the hub axis and rotating at the whirl speed Ω, the Reynolds equation for the flow in a plane journal bearing supporting a shaft of radius R, radial clearance C, rotational velocity ω and whirling eccentricity e (see Figure 4) becomes:

$$\frac{dp_0}{d\vartheta'} = -\frac{2\Lambda\dot{m}_0}{\rho\omega RH^3} + \frac{\Lambda\left(u_S + u_H\right)}{\omega RH^2}$$

with periodic boundary conditions $p\left(\vartheta'\right) = p\left(\vartheta' + 2\pi\right)$ for the pressure and constant mass flow in the bearing:

$$\dot{m}_0 = \int_R^{R+H} \rho u'_0 \, dr' = -\frac{\rho H^3}{12\mu R}\frac{dp_0}{d\vartheta'} + \frac{\rho H}{2}\left(u'_S + u'_H\right)$$

In the above equations, $\Lambda = 6\mu\omega R^2$ is the bearing number, $u'_H = -\Omega\left(R + C\right)$ is the hub velocity and, to the first order in the eccentricity, the height of the lubricating film is $H \cong C + e\cos\vartheta'$ and the shaft velocity is $u'_S \cong \left(\omega - \Omega\right)R + \Omega e\cos\vartheta'$. In addition, in infinitely long bearings either the supply pressure of the lubricant, p_{inj}, is specified at some appropriate location ϑ_{inj}, or the overall void fraction of the fluid film is assigned:

$$\bar{\alpha} = \frac{1}{2\pi RC}\int_{\vartheta}^{\vartheta+2\pi} \alpha HR\, d\vartheta$$

In high power density turbomachines the increase of the shaft speed, possibly combined with the use of low-viscosity lubricants, can raise the modified Reynolds number $\mathrm{Re}^* = \omega C^2/\nu_L$ of the bearing significantly above unity. In this case inertial effects in the lubricating fluid are no longer negligible. In the present work they have been included assuming that they represent a small correction of the Reynolds solution and can be approximated using the velocity field $\boldsymbol{u}_0$ obtained in the absence of the inertial forces (Kahlert's iteration method, 1947).

A single shooting method with fifth order Runge-Kutta integration and self-adaptive step size (Press *et al.*, 1992) has been chosen to numerically integrate the two points boundary value problem for the bearing flow, with or without corrections for inertial effects depending on the value of the modified Reynolds number Re^*. A modified multidimensional Newton-Raphson method has been used to iterate on the unknown initial conditions until the end-point boundary conditions are met with the required accuracy. The convergence and speed of the method remain excellent, even though they appreciably deteriorate in flows with extensive cavitation and low vapor pressure, especially at high Reynolds numbers and relative eccentricities.

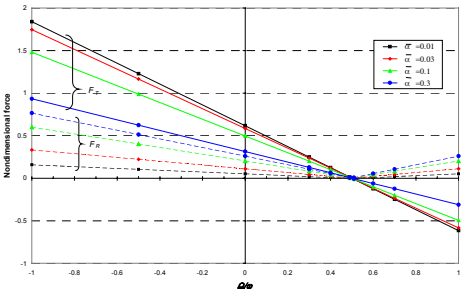

Figure 5. Radial and tangential rotordynamic forces, F_R (dashed lines) and F_T (solid lines), as functions of the whirl ratio Ω/ω for several values of the average void fraction $\bar{\alpha}$ and $\mathrm{Re}^* = 0.08$.

The two-phase flow model and the numerical scheme for the prediction of cavitation in journal bearings have been validated (Rapposelli and d'Agostino, 2001) against the experimental results by Floberg (1957). The agreement with the experimental data is quite satisfactory. More importantly for the validation of the proposed two-phase flow model, both the extent and shape of the pressure distribution in the cavitating region are accurately predicted by the isenthalpic approximation without the need for "ad hoc" assumptions.

Let consider first the behavior of whirling and cavitating bearings with negligible inertia of the lubricant ($\mathrm{Re}^* << 1$). In this case the effect of the whirl speed on the nondimensional radial and tangential rotordynamic forces, F_R and F_T, is shown in Figure 5. In the absence of cavitation ($\bar{\alpha} = 0$) the computations predict zero radial force and nearly linear tangential force, in accordance with known results for single-phase incompressible flows of constant vorticity $F_T = \varepsilon(1 - 2\Omega/\omega)$ (Vance 1988, Brennen 1994).

At finite void fractions, both the radial and tangential forces deviate appreciably from these results and display a more complex dependence on the whirl speed. The presence of vapor bubbles lowers the tangential force and generates a positive radial force, which increases rapidly with the void fraction and becomes comparable with the typical magnitude of the tangential force. The general features of the present solution at higher void fractions are consistent with the results of the π-approximation for cavitating bearings of low eccentricity (Vance 1988).

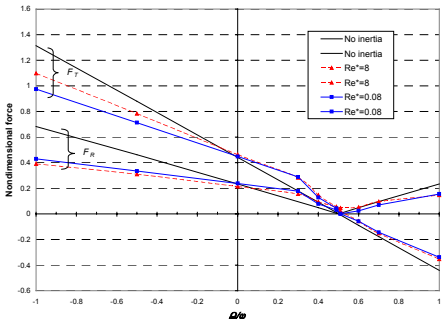

Figure 6. Radial and tangential rotordynamic forces, F_R and F_T, as functions of the whirl ratio Ω/ω in a whirling bearing with inertial effects (dots) and without inertial effects (solid lines). The modified Reynolds numbers are $\mathrm{Re}^* = 0.08 \text{ and } 8$.

It is worth recalling that rotordynamic forces are stabilizing when they tend to reduce the eccentricity and its whirl motion. Hence, with present notations and results, two-phase flow effects on the radial force are generally in favor of stability, but the tangential force remains destabilizing for whirl ratios Ω/ω ranging from 0 to about 0.5. In particular, consistently with the well-known features of the "oil whirl" instability (Newkirk and Taylor 1925, Hori 1959; Muszynska 1986), operation near $\Omega/\omega = 0.5$ is unstable because the eccentricity is not effectively controlled by the vanishing radial force and whirl motions can be sustained by the residual value of the tangential force. Notice that the extent of cavitation does not appreciably affect the "oil whirl" instability for $\Omega/\omega \cong 0.5$, but promotes stability for $0 < \Omega/\omega < 0.5$ by increasing the bearing stiffness and reducing the magnitude of the destabilizing tangential force.

Now consider the solution at moderate Reynolds numbers ($\mathrm{Re}^* > 1$). The influence of the inertial

effects on the bearing pressure distribution is illustrated in Figure 6 for some representative values of the whirl ratio. Except for the stationary case ($\Omega/\omega = 0$), comparison of the pressure profiles indicates that inertial effects significantly modify the pressure profile and the end point of the cavity, but have practically no influence on the inception location. The introduction of inertial effects reduces the bearing pressures at all whirl ratios but for the potentially unstable region $0 < \Omega/\omega < 0.5$ of the whirl spectrum, where the pressure profiles increase. Accordingly, for Reynolds numbers $\mathrm{Re}^* > 1$ the rotordynamic forces are higher than in the absence of inertial effects for $0 < \Omega/\omega < 0.5$, and smaller for the other whirl ratios. One can therefore conclude that for moderate Reynolds numbers ($\mathrm{Re}^* \cong 1 \approx 10$) the inertial effects effectively promote the rotordynamic stability of whirling and cavitating bearings. A second noteworthy aspect emerging from the above results is that even inertial effects that are practically undetectable in the stationary case ($\Omega/\omega = 0$) can nevertheless become quite significant in whirling bearings, because the eccentric motion effectively enhances the magnitude of the inertial forces developing in the lubricant.

Cavitating Hydrofoil Simulation

In this area of research Centrospazio has collaborated with CIRA (Centro Italiano Ricerche Aerospaziali) to the development of the two-phase flow model and the numerical code for simulating steady and unsteady cavitating flows in 2D configurations, both planar (hydrofoil) and axisymmetric (headforms). The simulation of cavitating flow requires the application of specialized methods because usual numerical schemes developed for compressible or incompressible flows are not capable of handling in a unified manner the simultaneous presence of extremely compressible cavitation pockets and practically incompressible fully-wetted flow regions separated by very rapid shock-like transitions. In view of these considerations, a pressure-based method based on the SIMPLE (Semi-Implict Method for Pressure-Linked Equations) algorithm has been chosen. With finite volume discretization in conservative form and Karki's compressibility correction, the method is shock-capturing and stable over a wide range of subsonic and supersonic Mach numbers, and has been tested with quite encouraging success in the analysis of cavitating flows in 2D axisymmetric and planar flow configurations (d'Agostino et al. 2001; Salvatore, Pascarella & d'Agostino, 2001).

The surface pressure distribution for incipient cavitation ($\sigma = 1$) on the modified NACA 66-109 hydrofoil at 4° incidence and $\mathrm{Re} = u_\infty c/\nu_L = 2 \cdot 10^6$ is presented in Figure 7. The simulations are in satisfactory agreement with the measured data by Shen and Dimotakis (1989) both in terms of the location and length of the cavitation region and the shape of the surface pressure profile. A sharp suction peak occurs at the leading edge, originating the formation of a cavitation region with practically constant pressure. The effect of increasing the temperature of the flow from 20 °C to 100 °C is illustrated in Figure 8. In the lack of reference experimental data, the quantitative assessment of thermal cavitation effects is hampered by the uncertain dependence of the parameter δ_T/R with the flow temperature. Comparison of Figures 7 and 8 indicates that at elevated temperatures:

- cavitation occurs for σ significantly smaller than $-C_{p\min}$ (thermal scaling);
- the length of the cavitation region decreases appreciably;
- the pressure in the cavitation region becomes less uniform and increases in the streamwise direction.

These findings are fully consistent with the limited available experimental evidence.

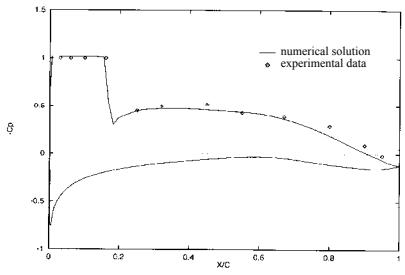

Figure 7. Comparison of the computed surface pressure coefficient (solid line) with the experimental data by Shen and Dimotakis, 1984 (dots) for developed cavitation in water on the modified NACA 66-109 hydrofoil. The flow conditions are: $\sigma = 1$, $T_L = 20°\mathrm{C}$, $\vartheta = 4°$ (angle of attack) and $\mathrm{Re}_c = 2 \cdot 10^6$.

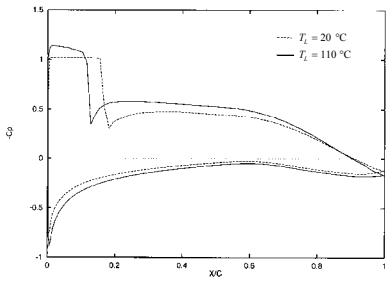

Figure 8. Comparison of the computed surface pressure coefficient for incipient cavitation in water on the modified NACA 66-109 hydrofoil at $T_L = 20$ °C (dotted line) and $T_L = 100$ °C (solid line). The flow conditions are: $\sigma = 1$, $\vartheta = 4°$ (angle of attack) and $\mathrm{Re}_c = 2 \cdot 10^6$.

Experimental Investigations

Experimental activities at Centrospazio mainly concerned on the design and the realization of the

CPTF (Cavitating Pump Test Facility) and its upgraded version, the CPRTF (Cavitating Pump Rotordynamic Test Facility). Extensive testing has demonstrated the effectiveness and versatility of the rig in experimentally characterizing turbopumps in a wide variety of alternative configurations (axial, radial, mixed flow, with or without an inducer).

The facility, operating in water at temperatures up to 90°C, is intended as a flexible apparatus that can readily be adapted to conduct experimental investigations on virtually any kind of fluid dynamic phenomena relevant to high performance turbopumps. The inlet section can be easily reconfigured allowing the accommodation of a Thermal Cavitation Tunnel (TCT) for experimentation on test bodies and hydrofoils.

Experimental Apparatus

The general configuration of the system is rather strictly constrained by its operational, economic and performance requirements and it is the result of an articulated work plan intended to resolution of technical problems and trade-offs in order to satisfy these requirements. Adjustable water pressure and temperature over relatively wide ranges, both above and below room conditions, are indispensable for controlling the extent and type (gaseous or vaporous) of cavitation. These are essential features for realistic simulation of turbopumps operating with fluids close to the saturation line, as commonly found in space propulsion applications. Together with the need of controlling cavitation nucleation and hardware corrosion by proper water treatment and additives, the above considerations virtually impose the choice of a closed, recirculating water loop with temperature, pressure, water quality, flow rate, rotation and eccentric whirl controls necessary for the pump to be tested under adjustable flux, load, speed, whirl and cavitation conditions.

Component Characteristics

The water loop hardware consists of the supporting structure, a 500 l air bag and heat exchanger, the suction and discharge piping, a series of auxiliary lines and tanks, two flow straighteners, two elastic couplings on the suction and discharge lines (to allow for vibration insulation, misalignment compensation and easy access and/or reconfiguration of the pump), a two-stage silent throttle valve for adjusting the pump load.

Motors and transmissions subsystem consists of a 30 kW brushless main motor (MOOG mod. FASF3V8029, $\Omega = 0 \div 3000$ rpm), and a 5.6 kW brushless whirl motor (MOOG mod. FASF2V4030, $\omega = 0, \pm 3000$ rpm), controlled by its power electronics in angular position and velocity with reference to the main motor, in order to retain a specified velocity ratio Ω/ω and initial/final angular positions during test runs. Two omokinetic couplings, the eccentric drive mechanism (Figure 9), the slip ring assembly (42 leads, Fabricast mod. 4200-1.498-42-36U), necessary to establish the electrical connections between the instrumented rotor (rotating dynamometer or other impeller-mounted sensors) and the stationary electronics (exciters, amplifiers and data acquisition).

The test section assembly (Figure 9) comprizes the pump housing and the transparent inducer casing. The pump housing essentially consists in a hollow aluminum cylinder rigidly mounted on the supporting structure and closed by two lids connected to the mechanism driving the shaft and with the transparent inlet duct. The rotating dynamometer is schematically illustrated in Figure 10. It is realized in a single piece of phase hardening steel AISI PH 17-4 and comprises two flanges connected by four square cross-section posts acting as flexing elements. Their deformation is sensed by 40 semiconductor strain gauges (Micron, mod. SS-060-033-500P-S4, 500 Ω, 140 gauge factor) arranged in 10 full bridges, which provide redundant measurements of the forces and moments acting on the impeller. Each bridge is temperature self-compensated and, for increased precision, has separate bipolar excitation and read-out.

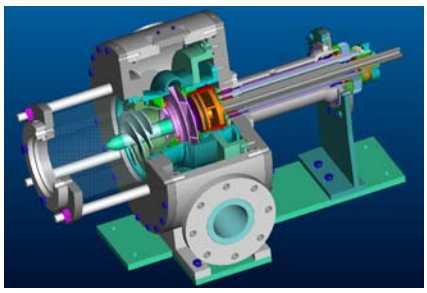

Figure 9. Assembly drawing of the CPRTF test section.

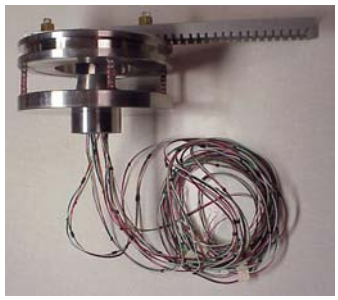

Figure 10. Rotating Dynamometer

The instrumentation consists in the rotating dynamometer, two electromagnetic flowmeters, (mod. 8705 Fisher-Rosemount), two absolute pressure transducers (Druck mod. PMP 1400, 0÷1 bar, 0.15% class and Kulite XTM-190M 0÷1.7 bar, 0.1% class), used on the inlet line to the pump for monitoring the suction pressure, and two piezoelectric pressure transducers (PCB M112A22, ICP® voltage mode-type, 0.1% class), used on the inlet line for used for dynamic analysis of unsteady

cavitation phenomena (rotating cavitation, auto-oscillation, cavitation surge, etc.). A high-speed data acquisition system, based on two 8-channel signal conditioning boards National Instruments mod. SCXI 1530, is used for the excitation, conditioning and acquisition of the 8 piezoelectric transducers. A medium-speed data acquisition system, based on an 16-channel signal conditioning board National Instruments mod. SCXI 1520 and a 250 kS/s acquisition board National Instruments mod. 6024E, is used for the other sensors.

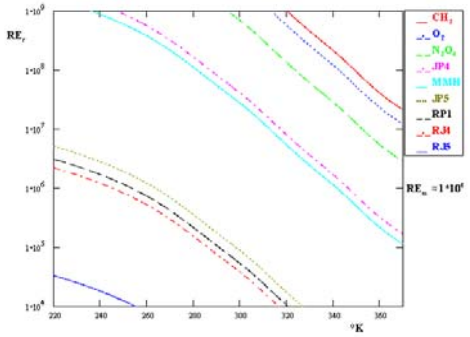

Figure 11. Thermal cavitation scaling in the CPRTF. Equivalent water temperature T_m required for scaling a pump prototype operating with different propellants at a given Reynolds number $\mathrm{Re}_r = 2\Omega r_T^2/\nu$. In all cases the Reynolds number of the pump model in the CPTF is $\mathrm{Re}_m = 10^6$.

CPRTF Operational Envelope

The operational characteristics of the facility have been chosen accounting for the need of retaining fluid dynamic and thermal cavitation similarity for accurate scaling of actual turbopumps, while still meeting stringent versatility, economic, maintenance and safety requirements. Fluid dynamic similarity requires that the full-scale prototype and the test model have equal shape, specific speed and cavitation number (Euler cavitation scaling), and equal Reynolds number (viscous and turbulent scaling). For thermal cavitation similarity, in both machines the time for a nucleus to develop thermally-controlled growth must be in the same ratio to its residence time in the turbopump.

The main operational parameters of the CPTF and RFTF are summarized in Tables 2 and 3. The resulting operational envelope of the CPRTF in terms of the nominal specific speed, Ω_{SS}, and diameter, d_S, of the machine covers with ample margins the parametric space occupied by axial, mixed, and radial flow turbopumps typically used in rocket propellant feed systems. The equivalent water temperature of a full-scale machine tested in the CPRTF at $\mathrm{Re} = 10^6$ is shown in Figure 11 as a function of the actual Reynolds number of the same machine operating with most common space propellants. The results confirm that thermal cavitation similarity in the CPRTF is attained at water temperatures safely lower than the boiling point.

Table 2. CPTF operational characteristics

Pump rotational speed	$\Omega = 0 \div 3000$ rpm
Main motor power	$P \le 30$ kW
Main motor torque	$M \le 100$ Nm
Suction pressure	$p_{t1} = 0.01 \div 6$ bar
Discharge pressure	$p_{t2} \le 11$ bar
Volumetric flow rate	$\dot{Q} \le 0.1 m^3/s$
Flow temperature	$T = 10 \div 90$ °C
Suction line diameter	DN = 6”
Discharge line diameter	DN = 4”
Impeller eye radius	$r_{T1} \le 90$ mm
Impeller outlet radius	$r_{T2} \le 112$ mm
Impeller outlet width	$b_2 \le 30$ mm

Table 3. RFTF operational characteristics

Adjustable eccentricity	$e = 0 \div 2$ mm
Whirl rotational speed	$\omega = -3000 \div 3000$ rpm
Nominal suspended mass	$m_S = 4$ kg
Dynamometer loads:	
lateral	$F_x = F_y \le 2400$ N
axial	$F_z \le 15000$ N
bending	$M_x = M_y \le 1400$ Nm
torque	$M_z \le 400$ Nm

Demonstration Tests

A set of demonstration experiments has been conducted on the CPTF and TCT using a commercial pump (with and without inducer) and a NACA 0015 hydrofoil, respectively. The nondimensional suction characteristics have been measured for the complete pump and the inducer alone. In particular, Figure 12 shows the behavior of the work coefficient $\psi = (p_{t2} - p_{t1}) / \rho\Omega^2 r_{T2}^2$ of a three-bladed helical inducer as a function of the Euler number, $\sigma = (p_1 - p_V) / \frac{1}{2}\rho A \Omega^2 r_{T1}^2$ for four different flow coefficients $\phi = \dot{Q} / \pi\Omega r_{T1}^3$. As expected, cavitation breakdown is delayed at higher values of the water temperature and the work coefficient increases slightly, reflecting the growing influence of thermal cavitation effects.

The influence of thermal cavitation effects on the flow instabilities has also been investigated by measuring the unsteady pressure fluctuations at the inlet section of the test pump and in the exit flow of the cavitating NACA 0015 hydrofoil (Rapposelli 2003). A global shift of all instability phenomena towards lower cavitation numbers has been observed at all flow coefficients as the flow temperature increases. This behavior has been only partially experienced in cryogenic fluids tests and simulations, and is likely related to the general delay of cavitation phenomena caused by thermal effects (Kato et al. 1996; Tani and Nagashima, 2002; Kamijo et al. 1993; Rebattet et al. 2002). The increase of the flow

temperature also increases both the cavitation volume and its stiffness. As indicated by the tenfold raise of the sonic speed at all void fractions when the temperature is raised from 20 to 70 °C (Figure 1), the latter effect is quite significant and probably dominant, leading to a generalized increase of the natural frequencies of the flow instabilities.

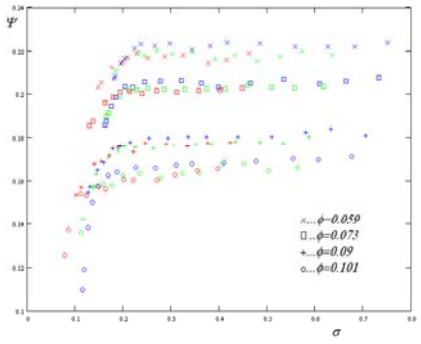

Figura 12. Suction characteristics of a three-bladed helical inducer ($\beta_T = 18°$, $r_T = 60$ mm, $r_H = 22$ mm) in water at $\mathrm{Re} = \Omega r_T^2 / \nu_L = 10^6$ and several flow coefficients and temperatures (– 25 °C;– 55 °C;– 75 °C).

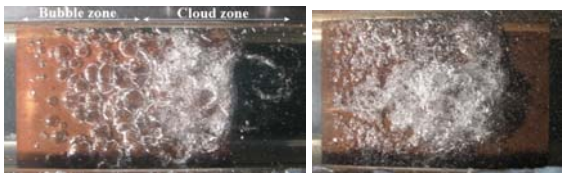

Figure 13. Typical cavitation appearance on NACA0015 hydrofoil in "Bubble+Cloud" case ($\alpha = 4°, \sigma = 1.25$, $T = 25°C$) and at higher freestream temperature ($\alpha = 8°, \sigma = 2$, $T = 70°C$).

A similar analysis on a NACA 0015 hydrofoil (Rapposelli et al. 2003), carried out with the aim of determining the behavior of the cavity length and oscillations at different incidence angles, cavitation numbers and freestream temperatures, also highlighted the presence of relevant thermal effects that considerably affect the wall pressure fluctuations measured about one chord downstream of the foil. Also in this case the changes of the pressure fluctuation spectra with the flow temperature can be qualitatively explained as the consequence of the increased stiffness of the cavities. "Solid blockage" effect due to the occurrence of cavitation also plays an important role in the process, by increasing the flow velocity and lowering the pressure on the suction side of the hydrofoil. Cavitation at higher freestream temperatures looks quite different: bubbles are smaller and tend to coalesce more easily, resulting in a narrower and less defined "bubble zone" compared to the "cloud zone" (Figure 13). Measured cavity length, surface pressure coefficients and unsteady pressure spectra are in good agreement with the data available in the open literature (Tsujimoto 1998; Kjeldsen et al. 1998; Tagaya et al. 199) and suggest the existence of a strong correlation between the onset of the various forms of cavitation-induced flow instabilities, thermal cavitation effects, and the influence of the tunnel walls.

Conclusions and Future Work

The results of recent work on cavitation modeling and simulation at Centrospazio confirm that the main features of thermal effects in cavitating flows can indeed be captured by the proposed model with proper choice of δ_T / R. Further experience with the application of the model to flows with well documented thermal cavitation effects is needed in order to obtain reliable estimates of δ_T / R in water and the other technical fluids of interest for accurate simulation of cavitating flows in rocket propulsion applications. To this purpose current numerical activities at Centrospazio and the Dipartimento di Ingegneria Aerospaziale, Università degli Studi di Pisa, are now geared toward the in-house development of a 3D, density-based, implicit, preconditioned code, which employs the above cavitation model on unstructured grids, optimized for flow analyses in the complex geometries typical of rocket propellant feed turbopumps.

At the same time Centrospazio is actively engaged in carrying out an intensive experimental activity on turbopumps cavitation with thermal effects, with particular attention to cavitation and related instabilities, whose results will contribute to provide useful data for better understanding the nature of these phenomena and for supporting ongoing modeling and simulation activities. This activity has been made possible through the realization of the CPRTF and its derivative configurations, a low-cost, versatile and easily instrumentable facility especially suited for carrying out experiments on cavitation-induced instabilities and rotordynamic forces in fluid dynamic and thermal cavitation similarity conditions.

Acknowledgements

The present work has been supported by the Agenzia Spaziale Italiana under the 1997 - 2000 contracts for fundamental research. The authors would like to acknowledge the help of all the students and colleagues who actively contributed to these activities (Mr. Angelo Cervone, Miss Cristina Bramanti, Mr. Andrea Milani, Mr. Roberto Merlo, Mr. Roberto Falorni, Dr. Fabrizio d'Auria and Mr. Marco Rosario Venturini Autieri) and express their gratitude to Profs. Mariano Andrenucci and Renzo Lazzeretti of the Dipartimento di Ingegneria Aerospaziale, Università degli Studi di Pisa, Pisa, Italy, for their constant and friendly encouragement.

References

Bhattacharyya A., 1994, "Internal Flows and Force Matrices in Axial Flow Inducers", Ph. D. thesis, Div. Eng. & Appl. Science, Caltech, Pasadena, CA, USA

Brennen C.E., 1994, "Hydrodynamics of Pumps", Concepts ETI, Inc. and Oxford University Press.

Brennen C. E., 1995, “Cavitation and Bubble Dynamics”, Oxford University Press.

d’Agostino L., & Venturini-Autieri M., 2002, “Three-Dimensional Analysis of Rotordynamic Fluid Forces on Whirling and Cavitating Finite-Length Inducers”, 9th Int. Symp. on Transport Phenomena and Dynamics of Rotating Machinery (ISROMAC-9), Honolulu, HI, USA, February 10-14.

d’Agostino L., Rapposelli E., Pascarella C. & Ciucci A., 2001, “A Modified Bubbly Isenthalpic Model for Numerical Simulation of Cavitating Flows”, AIAA Paper 2001-3402.

Floberg L., 1957, Trans. Chalmers Univ. of Technology, Vol. 189, Götheburg, Sweden.

Goirand B., Mertz A.L., Jousselin F. & Rebattet C., 1992, "Experimental Investigations of Radial Loads Induced by Partial Cavitation with Liquid Hydrogen Inducer", IMechE, C453/056, pp. 263-269.

Hori Y., 1959, “The Theory of Oil Whip”, ASME J. Appl. Mech., Vol. 26, pp. 189-198.

Kahlert W., 1947, Ingr.Archiv, Vol. 16, pp. 321-342.

Kamijo K., Yoshida M. & Tsujimoto Y., 1993, "Hydraulic and Mechanical Performance of LE-7 LOX Pump Inducer", ASME J. Propulsion and Power, Vol. 9, No. 6, pp. 819-826.

Kamijo K., Shimura T. & Tsujimoto Y., 1993, "Experimental and analytical study of rotating cavitation", ASME FED-190, pp. 33-43.

Kato H., Maeda M., Kamono H. & Yamaguchi H., 1996, “Temperature Depression in Cavity”, Fluids Engineering Division Conference, San Diego, USA, July 7-11

Kjeldsen M., Effertz M. & Arndt R.E.A., 1998, “Investigation of Unsteady Cavitation Phenomena”, Proc. of US-Japan Seminar: Abnormal Flow Phenomena in Turbomachinery, Osaka, Japan, Nov. 1-6

Mori A. & Mori H., 1991, “Re-Examination of Film Rupture Boundary Condition in Hydrodynamic Lubrication under Inertia Effect”, ASME J. of Tribology, Vol. 113, pp. 604-608.

Muster D. & Sternlicht B., ed., 1965, Proc. Int. Symp. on Lubrication and Wear.

Muszynska A., 1986, “Whirl and Whip Rotor/Bearing Stability Problems”, J. Sound and Vibrations, Vol. 110, pp. 443-463.

Newkirk B.L. and Taylor H.D., 1925, “Shaft Whipping due to Oil Action in Journal Bearing”, General Electric Review, August, pp. 559-568.

NASDA, 2000a, Report No. 94, May 2000.

NASDA, 2000b, Report No. 96, June 2000.

Press W. et al., 1992, “Numerical Recipes in FORTRAN”, Cambridge University Press, 2nd Edition.

Rapposelli E. & d’Agostino L., 2001, “A Modified Isenthalpic Model of Cavitation in Plane Journal Bearings”, CAV2001, International Symposium on Cavitation, Pasadena, California USA, June 20-23.

Rapposelli E., Falorni R. & d’Agostino L., 2002, "Two-Phase and Inertial Effects on the Rotordynamic Forces in Whirling Journal Bearings", Proc. 2002 ASME FED Summer Meeting, Montreal, Quebec, Canada, July 14-18.

Rapposelli E., Cervone A., Bramanti C. & d’Agostino L., 2002, “A New Cavitation Test Facility at Centrospazio”, 4th Int. Conf. on Launcher Technology, Liege, Belgium, Dec. 3-6.

Rapposelli E., Cervone A., Bramanti C. & d’Agostino L., 2003, “Thermal Cavitation Experiments on a NACA 0015 Hydrofoil”, 4th ASME_JSME Joint Fluids Engineering Conference, Honolulu, USA, July 6-10.

Rapposelli E., 2003, “Theoretical and Experimental Analysis of Cavitation Phenomena in Turbopumps for Space Applications”, Ph.D. thesis, Pisa Univ., Pisa, Italy.

Rebattet C., Franc J. P., Riondet M., Coulon A., Bonhomme C., 2002, “Investigation of Thermodynamic Effect in Cavitating Inducers an Experimental Study on French University Facilities”, 4th Int. Conf. on Launcher Technology, Liege, Belgium, Dec. 3-6.

Reinhardt E. & Lund J.W., 1975, “The Influence of Fluid Inertia on the Dynamic Properties of Journal Bearings”, ASME J. Lubrication Technology, Vol. 97, Sez. F, pp. 159-167.

Ryan R.S., Gross L.A., Mills D. & Michell P., 1994, "The Space Shuttle Main Engine Liquid Oxygen Pump High-Synchronous Vibration Issue, the Problem, the Resolution Approach, the Solution", AIAA Paper 94-3153.

Salvatore V., Pascarella C. & d’Agostino L., 2001, “Numerical Evaluation of Cavitating Flows Using Different Two-Phase Models”, ICMF2001 Paper 713, New Orleans, Luoisiana USA, June.

Shen Y.T. & Dimotakis P.E., 1989, “The Influence of Surface Cavitation on Hydrodynamic Forces”, Proc. 22nd ATTC, St. Johns.

Stripling L.B. and Acosta A.J., 1962, "Cavitation in Turbopumps – Part 1, ASME J. Basic Eng., Vol. 84, pp. 326-338.

Swales P.D., 1975, “A Review of Cavitation Phenomena In Engineering Situations”, 1st Leeds-Lyon Int. Symp. on Trib., pp. 3-9.

Tagaya Y., Kato H., Yamaguchi H., Maeda M., 1999, “ Thermodynamic Effect on a Sheet Cavitation”, ASME/JSME FEDSM, S. Francisco, California, July 18-23

Tani N. and Nagashima T., 2002, “Numerical Analysis Of Cryogenic Cavitating Flow On Hydrofoil – Comparison Between Water and Cryogenic Fluids”, ”, 4th Int. Conf. on Launcher Technology, Liege, Belgium, Dec. 3-6.

Tsujimoto Y., Semenov Y. A., 2002, "New Types of Cavitation Instabilities in Inducers", 4th Int. Conf. on Launcher Technology, Liege, Belgium, Dec. 3-6.

Tsujimoto Y., Watanabe S., Horiguchi H., 1998, “Linear Analyses of Cavitation Instabilities of Hydrofoils and Cascades”, Proc. of US-Japan Seminar: Abnormal Flow Phenomena in Turbomachinery, Osaka, Japan, Nov. 1-6

Tsujimoto Y., Yoshida Y., Hashimoto T.,1997, "Observation of Oscillating Cavitation of an Inducers", ASME J. Fluids Eng. ing, Vol. 119, pp. 775-781.

Vance J.M., 1988, “Rotordynamics of Turbomachinery”, John Wiley & Sons, New York, USA.

Zoladz T., 2002, *personal communication*.